Original Article

LncRNA MALAT1 induced by hyperglycemia promotes microvascular endothelial cell apoptosis through activation of the miR-7641/TPR axis to exacerbate neurologic damage caused by cerebral small vessel disease

Fei Che[1], Yunfeng Han[2], Jinxia Fu[1], Nannan Wang[1], Yuehui Jia[2], Kun Wang[1], Jie Ge[2]

[1]The Second Ward of the Department of Neurology, The Second Affiliated Hospital of Qiqihar Medical University, Qiqihar, China; [2]Department of Epidemiology and Statistics, School of Public Health, Qiqihar Medical University, Qiqihar, China

Contributions: (I) Conception and design: F Che, J Ge, Y Han; (II) Administrative support: J Fu; (III) Provision of study materials or patients: N Wang, K Wang, F Che; (IV) Collection and assembly of data: J Ge, F Che; (V) Data analysis and interpretation: Y Han, Y Jia; (VI) Manuscript writing: All authors; (VII) Final approval of manuscript: All authors.

Correspondence to: Jie Ge. Department of Epidemiology and Statistics, School of Public Health, Qiqihar Medical University, No. 333 Bukui Street, Jianhua District, Qiqihar 161006, China. Email: gejie_submit@163.com.

Background: This study aimed to explore the effect of hyperglycemia-induced long noncoding RNA (lncRNA) metastasis-associated lung carcinoma transcript 1 (MALAT1) on microvascular endothelial cell activity. In addition, we investigated the possible downstream molecular regulatory mechanism in order to provide an adjunctive therapeutic target for the prognostic nerve recovery of cerebral small vessel disease (CSVD).

Methods: A rat model of diabetes was induced by streptozotocin (STZ) injection in combination with a high-energy diet. The mixed model of CSVD and hyperglycemia was prepared by injection of homologous microemboli in vitro. Results of 3-(4,5-dimethylthiazol-2-yl)-2,5 diphenyltetrazolium bromide (MTT) assay and enzyme-linked immunosorbent assay (ELISA) showed that the inhibition of lncRNA MALAT1 by siRNA in a high-glucose environment effectively alleviated the cell damage caused by high glucose (HG) and reduced the rate of apoptosis. We found that the upregulation of downstream miR-7641 and TPR (translocated promoter region) reduced the occurrence of cell damage and apoptosis.

Results: The results of neurological deficit score showed that the scores of ICH group, HG group and HG + ICH group were significantly higher than those of Sham group, and the differences were statistically significant. The qPCR results showed that the MALAT1 level of the model group was significantly different from that of the sham group, and the expression levels of damage markers vWF and ICAM-1 were detected by Western blot (WB), which were significantly higher in the model group than in the sham group. The MTT cell activity assay showed that the addition of miR-7641 inhibitor or TPR short hairpin RNA (shRNA) into normally cultured cells reduced cell activity. ELISA results showed that low expression of miR-7641 increased the apoptosis rate of microvascular endothelial cells. Western blot (WB) results showed that the protein expression levels of BAX and cleaved caspase-3 (c-caspase-3) were negatively correlated with miR-7641. The regulation of TPR expression showed similar results.

Conclusions: High blood glucose level induced the increase of lncRNA MALAT1 and regulated the expression of TPR by activating miR-7641 to promote the initiation of apoptosis of microvascular endothelial cells, aggravating the neurological dysfunction caused by CSVD.

Keywords: Cerebral small vessel disease (CSVD); hyperglycemia; long noncoding RNA metastasis-associated lung carcinoma transcript 1 (lncRNA MALAT1); apoptosis

Submitted Oct 15, 2021. Accepted for publication Dec 14, 2021.
doi: 10.21037/atm-21-5997
View this article at: https://dx.doi.org/10.21037/atm-21-5997

Introduction

Cerebral small vessel disease (CSVD) is a common cerebrovascular disease. The complications and poor prognosis of CSVD lead to substantial financial pressure and mental burden on patients and their families. Previous studies have found that CSVD in diabetic patients resulted in more serious clinical manifestations (1-3), and higher blood glucose levels had a negative impact on the prognosis of CSVD (4,5). However, the mechanism of its occurrence and development remains unclear. A large number of studies have confirmed that hyperglycemia affects the physiological activity of vascular endothelial cells (6,7) and damages the normal function of vascular endothelial cells, enhancing permeability and aggravating cerebral edema. Studies have shown that diabetic patients are more likely to suffer from mitochondrial dysfunction of vascular endothelial cells after CSVD (8,9). In addition, high blood glucose level could activate the immune system, stimulate the phenotype transformation of macrophages, activate the expression of inflammatory factors such as *s*ignal transducer and activator of transcription 3 (STAT3) and suppressor of cytokine signaling 3 (SOCS3), cause immune-mediated small vessel disease and nerve cell damage, and affect higher neurological function. It has been found that hyperglycemia affects the dedifferentiation of brain pericytes through the p21-SOX2 signaling pathway (10,11).

Long noncoding RNA (lncRNA) plays an important role in the pathophysiological process of CSVD. A large number of studies have reported that lncRNA participated in multiple stages of cerebral injury and played an important regulatory role in the activation of inflammatory, oxidative stress, and other signaling pathways (12-15). LncRNA has also been found to participate in the process of proliferation, differentiation, aging, apoptosis, and angiogenesis of endothelial cells, and play an important role in regulating vascular endothelial function (16-20). For example, lncRNA metastasis suppressor 1 (MTSS1) is involved in regulating the expression of *phosphorylated* p65 (*p-p65*), tumor necrosis factor α (TNF-α), and interleukin-1 (IL-1), aggravating inflammatory response after CSVD (15). Brown fat lncRNA 1 (Blnc1) regulates vascular permeability by mediating the peroxisome proliferator activated receptor γ (PPAR-γ)/sirtuin 6 (SIRT6)/forkhead box O3 (FOXO3) pathway, and downregulation of Blnc1 can improve CSVD-induced edema and inflammation (21). LncRNA metastasis-associated lung carcinoma transcript 1 (MALAT1) was first identified for its ability to regulate autophagy and inflammation, and the expression of MALAT1 has been shown to be significantly upregulated in an endothelial cell ischemia-reperfusion model. Studies have found that lncRNA MALAT1 was able to protect brain microvascular endothelial cells from injury caused by oxygen-glucose deprivation/reoxygenation by upregulating the expression of autophagy promoter unc-51-like autophagy activating kinase 2 (ULK2) (22). At the same time, MALAT1 can be used as a marker and therapeutic target for the diagnosis and treatment of complications and prognosis assessment related to diabetes mellitus (DM) (23). MALAT1 mediates the production of glucose-induced inflammatory cytokines, including TNF-α and IL-6 in endothelial cells, and aggravates DM-related vascular injury. In a DM ischemia-reperfusion model, MALAT1 was found to upregulate the expression of myeloid differentiation primary response 88 (MyD88) adaptor protein, TNF receptor-associated factor 6 (TRAF6), and IL-1 receptor-associated kinase 1 (IRAK1), activating the nuclear factor-κ*B* (NF-κB) cascade reaction and promoting the occurrence of cerebral ischemia-reperfusion injury (24). LncRNA MALAT1 plays an important role in DM. In this study, small interfering RNA (siRNA) was constructed to regulate the expression of lncRNA MALAT1 in endothelial cell lines in a high-glucose environment in order to explore the effect of blood glucose level on endothelial cells after CSVD and its mechanism, thereby providing a reference for the prognosis and treatment of CSVD.

We present the following article in accordance with the ARRIVE reporting checklist (available at https://dx.doi.org/10.21037/atm-21-5997).

Methods

Experimental animals

A total of 65 specific-pathogen free (SPF) 8-week-old male Sprague Dawley (SD) rats (250±20 g) were used in

this study. The rats were purchased from Guangdong Medical Laboratory Animal Center and raised at 22 ℃ with 60% humidity and a 12-hour light and dark cycle. The animals were given food and water was available ad libitum. Animal experiments were approved by the Animal Ethics Committee of Qiqihar Medical University (No. QMU-AECC-2020-66), in compliance with Guidelines for the Ethical Review of Laboratory Animal Welfare (GB/T 35892-2018) for the care and use of animals.

Animal grouping and model preparation

In this study, 5 experimental groups were set up: the normal group (Nor), sham operation group (Sham), CSVD group, hyperglycemia group (HG), and CSVD with hyperglycemia group (CSVD+HG). The normal group contained 5 rats and the remaining 4 groups contained 15 rats each. Before the experiment, the rats were numbered in order of weight, the same number was selected from the random number table to match the initial number, and then the random number was divided by 5 and grouped according to the remainder. No treatment was performed on the normal group. The hyperglycemic group was fed high-glucose and high-fat food for 4 weeks, followed by a single intraperitoneal injection of 1.75% streptozotocin (STZ) sodium citrate buffer at 35–50 mg/kg. Seventy-two hours after STZ injection, all rats were fasted for 12 hours, and a 20% glucose solution was administered by oral gavage at a dose of 2.0 g/kg to conduct an oral glucose tolerance test (OGTT). Rats with fasting blood glucose (FBG) ≥7.8 mmol/L or peak blood glucose ≥16.7 mmol/L indicated successful modeling, and the CSVD model was prepared. Left ventricular blood of the rats from the same strain was collected, dried, aseptically coagulated at 80 ℃, and then ground. The ground blood was then screened with 200 μm mesh and dissolved in normal saline to prepare a 30 mg/mL microemboli suspension. The CSVD model was made with microembolus injection *in vitro*. The rats were anesthetized with 3% pentobarbital sodium at a dose of 0.15 mL/100 g. The rats were fixed on the operating table in supine position, and the neck skin was disinfected for draping. A midline neck incision was performed. The left common carotid artery, internal carotid artery, and external carotid artery were bluntly separated. The proximal end of the common carotid artery and the distal end of the external carotid artery were briefly occluded, and a reverse intubation was performed on the external carotid artery to inject 0.3 mL microembolus suspension. Upon injection, the common carotid artery was immediately opened, the proximal end of the external carotid artery was ligated, and the wounds were sutured in turn. If the rats woke and did not show abnormal movement such as epilepsy, the modeling was deemed successful. Neurologic impairment was evaluatednbased on the classic Bederson scale (0–4 points). The higher the score, the worse the neurological impairment.

Cell culture and treatment

In this study, the *in vitro* subject was microvascular endothelial cell line hCMEC/D3, which was purchased from Otwo Biotech (Shenzhen, China). The cells were inoculated into a culture dish coated with collagen IV and cultured at 37 ℃ and 5% CO_2. The normal cell culture medium was endothelial basal medium (EBM)-2 with 20% *fetal bovine serum* (FBS) and 100 U/mL penicillin streptomycin (1:1). The hyperglycemia group was cultured with 35.0 mM glucose culture medium, and the solution was changed every 24 hours. Hypoxic-treated cells were cultured in a hypoxic chamber (95% N_2 and 5% CO_2) for 12 hours. Cells in the control group were cultured under normal conditions. The cells in each group were collected for analysis of the expression of related genes using reverse transcription polymerase chain reaction (RT-PCR).

Cell activity analysis

Cell activity was assessed using the Beyotime 3-(4,5-dimethylthiazol-2-yl)-2,5 diphenyltetrazolium bromide (MTT) cell activity analysis kit (Beyotime Biotechnology, Shanghai, China). MTT (25 mg) was dissolved with 5 mL MTT solvent to prepare 5 mg/mL MTT solution. HCMEC/D3 cells were inoculated into the 96-well plate at a density of 2,000 cells/well, 10 μL MTT solution was added to each well, and the cells were incubated for 4 hours. Formazan solution (100 μL) was added to each well and the cells were incubated at 37 ℃ for about 3–4 hours until all purple crystals had dissolved. The light absorption value of each well was measured at optical density (OD) 570 nm using an enzyme-linked immunosorbent assay (ELISA). The results were recorded and the corrected absorbance value was obtained by subtracting the mean value of blank wells from all absorbance values. The mean value of cells in the normal group was taken as the baseline (100%) and cell activity (%) = [OD/standard deviation $(SD)_{OD\ (Nor)}$] *100.

Apoptosis assay

We used the apoptosis assay ELISA Kit (Sigma-Aldrich, St Louis, MO, USA) to quantify mononuclear oligomeric nucleosomes (histone-related DNA fragments). As directed by the manufacturer's instructions, the cells were incubated with incubation buffer for 18 hours, and then the cell lysate was added. The cytosol protein was adsorbed into the pores of the streptavidin-coated plate. A mixture of antihistamine-biotin and anti-DNA-POD antibody was added to the cell lysates and incubated for 2 hours. After the cells were washed with phosphate-buffered saline (PBS), ELISA stop solution was added to each well. The light absorption value of each well was measured with ELISA at OD 570 nm, and blank correction was performed for all obtained data.

Western blot (WB)

WB analysis was used to determine the protein expression. The extraction of total protein was quantified with lysate buffer containing protease and phosphatase inhibitors (Beyotime) and a bicinchoninic acid (BCA) assay kit (Beyotime). The cells were separated by sodium dodecyl sulphate-polyacrylamide gel electrophoresis (SDS-PAGE), transferred to polyvinylidene difluoride (PVDF) membranes (PerkinElmer Billerica, MA, USA), and then incubated with specific antibodies for 12 hours at 4 ℃. The antibodies included anti-glyceraldehyde 3-phosphate dehydrogenase (GAPDH) antibody [6C5]-Loading Control (ab8245) (1:1,000), anti-von Willebrand factor (vWF) antibody [EPR12011] (ab174290) (1:2,000), anti-intercellular adhesion molecule-1 (ICAM1) antibody [EPR16608] (ab179707) (1:1,000), anti-Bcl-2 antibody (ab196495) (1:1,000), anti-caspase-3 antibody [31A1067] (ab13585) (1:50), anti-Akt antibody (ab8805) (1:500), anti-Akt (phospho T308) antibody (ab38449) (1:1,000), anti-GSK3 beta antibody (ab93926) (1:1,000), and phosphorylated glycogen synthase kinase 3 beta (p-GSK3β) (Ser9) (1:1,000, cat no. 9336, CST). The membrane was then incubated with secondary immunoglobulin G (IgG) antibody bound to horse radish peroxidase (HRP) for 2 hours. Enhanced chemiluminescence (Thermo Fisher Scientific, Waltham, MA, USA) was used to detect the target protein, and the band intensity was quantified and standardized according to the load control. The antibodies used in this study were purchased from Abcam and CST and they were used and stored according to the manufacturers' instructions.

Quantitative (q)-PCR

The expression level of target messenger RNA (mRNA) was analyzed by real-time quantitative PCR. TRIZOL reagent (Sigma-Aldrich) and RNeasy Mini Kit (Sigma-Aldrich) were used to extract total RNA from samples. Complementary DNA (cDNA) was synthesized with Omniscript reverse transcription (RT) kit (QIAGEN, Hilden, Germany) and qPCR was amplified with SYBR Green (QIAGEN). The CFX96 system (Bio-Rad Laboratories, Hercules, CA, USA) was used for quantitative analysis of RT-qPCR gene expression. Each real-time PCR sample (10 μL) contained 1 μL cDNA and 5 μL SYBR Green (QIAGEN), and the final concentration of forward and reverse primers was 10 μM.

All reactions were carried out at 95 ℃ for 10 minutes, then denatured at 95 ℃ for 2 seconds, annealed at 60 ℃ for 20 seconds, and extended at 70 ℃ for 10 seconds. Forty cycles were performed. A melt curve was produced as temperature was increased from 70 ℃ to 95 ℃ in 0.5 ℃ increments within 5 seconds to ensure specificity of amplification. Taking GAPDH as reference, the relative expression level was calculated using the ΔΔCt method. The primer sequences are shown in *Table 1*.

Bioinformatics analysis

In this study, the Encyclopedia of RNA Interactomes (ENCORI) (http://rna.sysu.edu.cn/encori) tool in starBase (http://starbase.sysu.edu.cn/index.php) was used to analyze and predict RNA-RNA and RNA-DNA interactions.

LncRNA-RNA

The human genome version 19 (hg19) was selected, MALAT1 was entered in the gene search box, and microRNAs (miRNAs) were screened from the search results. The results were displayed by number of action sites and miR-7641 was selected as the study object.

Target gene prediction of miRNA-7641

Hg19 was selected, miR-7641 was entered into the miRNA search box, and using the gene type "protein coding", gene IDs were screened from the results. The Search Tool for the Retrieval of Interacting Genes/Proteins (STRING) database was used to construct a target gene protein interaction network and Gene Ontology (GO) enrichment

Table 1 Primer sequences

Primer	Forward primer	Reverse primer
GAPDH	5'-GAAAGCCTGCCGGTGACTAA-3'	5'-GCATCACCCGGAGGAGAAAT-3'
lncRNA MALAT1	5'-ACTTCTGAATGAGGCTTCAG-3'	5'-UGAAGCGCCGCGTGTTTAAACG-3'
miR-7641	5'-TTGATCTCGGAAGCTAAGC-3'	5'-AAGCTCTATTGACCTGGAT-3'
TPR	5'-AACGCCAGCGTGAGGAATATG-3'	5'-ATTACGTGGTTACCCCTTGCT-3'

GAPDH, glyceraldehyde-3-phosphate dehydrogenase; mTPR, mRNA translocated promoter region.

analysis was performed.

Regulation of the expression level of target molecules

Regulation of lncRNA MALAT1 expression

The siRNA used in this study inhibited the expression of lncRNA MALAT1, and siMALAT1 (5'-GAAUUCCGGUGAUGCGAGU-3') was purchased from GenePharma (Shanghai, China). HCMEC/D3 cells were inoculated into the 6-well plate at a density of 1×10^5 cells per well. Lipofectamine 2000 (Invitrogen, Waltham, MA, USA) was then used to dilute lncRNA MALAT1 siRNA and control siRNA (SIR-C) to 500 nM for transfection. The knockdown efficiency of lncRNA MALAT1 was measured by qPCR after 48 hours. One-way ANOVA was used for the PCR results of siRNA and siR-C and $P<0.001$, indicating that the siRNA purchased met the experimental conditions.

Regulation of miR-7641 expression

MiR-7641 mimics, miR-7641 inhibitors, and miRNA negative control (NC) used in this study were provided by GenePharma (Shanghai). According to the manufacturer's instructions, miRNA mimic (1.25 μL, 20 μM) was diluted with 30 μL 1× riboFECT™ CP Buffer (30 μL), riboFECT™ CP Reagent (3 μL) was added, and the mixture was incubated at room temperature for 10–15 min. The mixture was then added to the protocell medium and the transfection concentration was 50 nM.

Regulation of translocated promoter region (TPR) expression

In this study, short hairpin RNA (shRNA) was used to silence TPR expression. TPR shRNA (5'-CTCAAGATT CCATTGGAGAAGGAGTTACC-3') was provided by GenePharma (Shanghai) and the Lipofectamine 3000 Kit (Thermo Fisher) was used for transfection. The cells were inoculated into the 6-well plate at 5×10^5 cells/well, and Lipofectamine 3000 (100:6) and DNA (50:1) were diluted with serum-reducing medium. Lipofectamine 3000 was mixed with DNA dilution in equal volumes and incubated at room temperature for 10–15 min. Next, 250 μL of the mixture was added to each well and cultured at 37 ℃ for 48 hours. Proteins and RNA were extracted for subsequent detection.

In order to verify the effect of TPR on pathways of apoptosis, enhanced green fluorescent protein (EGFP)-TPR overexpression plasmid was used to conduct cell transfection. The expression vector of EGFP-TPR was provided by Addgene (Waterton, MA, USA), and the full-length TPR gene was cloned into pEGFP-N1 vector to construct the overexpressed plasmid. The cells were inoculated into the 6-well plate at 5×10^5 cells/well, and Lipofectamine 3000 (100:6) and DNA (50:1) were diluted with serum-reducing medium. P3000 was added to the DNA diluent at a volume of 2 μL/μg DNA and the solution was mixed well. Then, Lipofectamine 3000 and the DNA diluent were mixed in equal volumes and incubated at room temperature for 10–15 minutes. Next, 250 μL of DNA-liposome complex was added to each well. Cells were cultured at 37 ℃ for 48 hours. Proteins and RNA were extracted for subsequent detection.

Statistical analysis

The data were analyzed with GraphPad prism 8 software, and all quantitative data are expressed as the mean ± standard deviation (Standard Deviation, SD) of at least 3 samples. In order to ensure the reproducibility of experimental results, each group of experiments was repeated independently at least 3 times. Statistical differences between groups were determined by 1-way analysis of variance, and $P<0.05$ indicated statistical significance.

Results

Hyperglycemia aggravates neurologic impairment caused by CSVD

In order to explore the effect of hyperglycemia on cerebrovascular injury, we evaluated the neurologic impairment in the normal group (Nor), Sham group (Sham), cerebral small vascular disease (CSVD) group, hyperglycemia group (HG), and CSVD with hyperglycemia group (CSVD + HG) at 6 hours, 24 hours, and 72 hours, respectively. The results are shown in *Figure 1A*. Different degrees of neurological dysfunction appeared in each model group at 24 hours, and the difference tended to be stable after 72 hours. The results showed that compared with the Sham group, the hyperglycemia group showed more obvious neurologic impairment at 24 hours (P<0.01), with no significant improvement observed at 72 hours. Compared with the CSVD group, the CSVD + HG group showed more serious neurologic impairment (P<0.01). The cerebral vascular endothelial cells of rats in each group were then extracted to detect the expression level of damage markers vWF and ICAM1. WB results showed that protein levels of vWF and ICAM1 in the hyperglycemia group were significantly higher (P<0.01) than those in the Sham group, and expression levels of damage markers in the CSVD + HG group were the highest (*Figure 1B*). In order to further explore the mechanism of hyperglycemia on neurologic impairment, we reviewed relevant research from home and abroad, and we speculated that lncRNA MALAT1 might play an important role. Primary cerebral microvessels were then extracted to detect the expression of lncRNA MALAT1 in each group (*Figure 1C*). Q-PCR results showed that lncRNA MALAT1 was significantly increased in both hyperglycemia and CSVD conditions (Sham *vs.* HG, P<0.01; Sham *vs.* CSVD, P<0.01). The level of lncRNA MALAT1 was the highest in the CSVD + HG group, which had the highest degree of neurologic impairment (Sham *vs.* CSVD + HG, P<0.001). These results suggested that higher blood glucose levels may have affected neurological function by upregulating lncRNA MALAT1expression.

Downregulation of lncRNA MALAT1 can alleviate the apoptosis of microvascular endothelial cells

The microvascular endothelial cells cultured under conditions of hypoxia were used as a model for *in vitro* investigation of CSVD. RT-PCR results showed that the expression level of lncRNA MALAT1 in cells cultured under high glucose (HG) or oxygen deficit (OD) conditions was higher than that in normal group (Nor) and lower than that in high glucose + oxygen deficit (HG + OD) group (*Figure 2A*). In order to study the correlation between lncRNA MALAT1 level and microvascular endothelial cell damage, the expression level of lncRNA MALAT1 in microvascular endothelial cells was regulated by siRNA. Based on qPCR verification, the transfection regulation effect met the experimental requirements (*Figure 2B*). The transfected cells were cultured in a HG environment for 48 hours, and cell activity was detected by MTT. The results (*Figure 2C*) showed that a HG culture environment significantly affected the cell activity (HG *vs.* Nor, P<0.001). Downregulation of lncRNA MALAT1 expression reduced the effect of HG on cell activity (HG + siMALAT1 *vs.* HG + NC, P<0.01). Subsequently, ELISA was used to detect the level of apoptosis in each group. The results (*Figure 2D*) showed that HG significantly increased apoptosis (HG *vs.* Nor, P<0.001), while inhibition of lncRNA MALAT1 significantly decreased apoptosis (HG + siMALAT1 *vs.* HG + NC, P<0.001). According to the WB assay, the expression levels of apoptosis markers, including BAX, BCL2, and cleaved caspase-3 (c-caspase-3) (*Figure 2E*), were significantly increased (HG *vs.* Nor, P<0.01), while the expression levels of anti-apoptosis-related proteins were significantly decreased (HG *vs.* Nor, P<0.01) under HG conditions. Protein levels in the lncRNA MALAT1-inhibited group were somewhat regulated (HG + siMALAT1 *vs.* HG + NC, P<0.01). The above experimental results indicated that, to a certain extent, downregulation of lncRNA MALAT1 alleviated of microvascular endothelial cell damage caused by HG.

Downregulation of lncRNA MALAT1 may play a role through miR-7641

In order to further explore the mechanism of lncRNA MALAT1, ENCORI was used to predict the downstream factors of lncRNA MALAT1. The screened results showed that miR-7641 and miR-4485 may play a role as downstream factors of lncRNA MALAT1 (*Figure 3A*). A literature review revealed that miR-7641 played an important role in maintaining vascular stability. In order to investigate whether miR-7641 would be affected by a HG environment, the expression levels of miR-7641 in the normal group, HG group, lncRNA MALAT1-inhibited group and control group were detected (*Figure 3B*). The results showed that miR-7641

A

Group	n	6 h	24 h	72 h
Nor	15	0.00±0.00	0.00±0.00	0.00±0.00
Sham	15	0.93±0.30	0.91±0.35	0.00 ±0.00
CSVD	15	2.06±0.19	2.23±0.32	2.57±0.32
HG	15	1.50±0.14*	1.77±0.27**	1.76±0.22**
HG + CSVD	15	2.00±0.55#	2.85±0.55#	3.2±0.36#

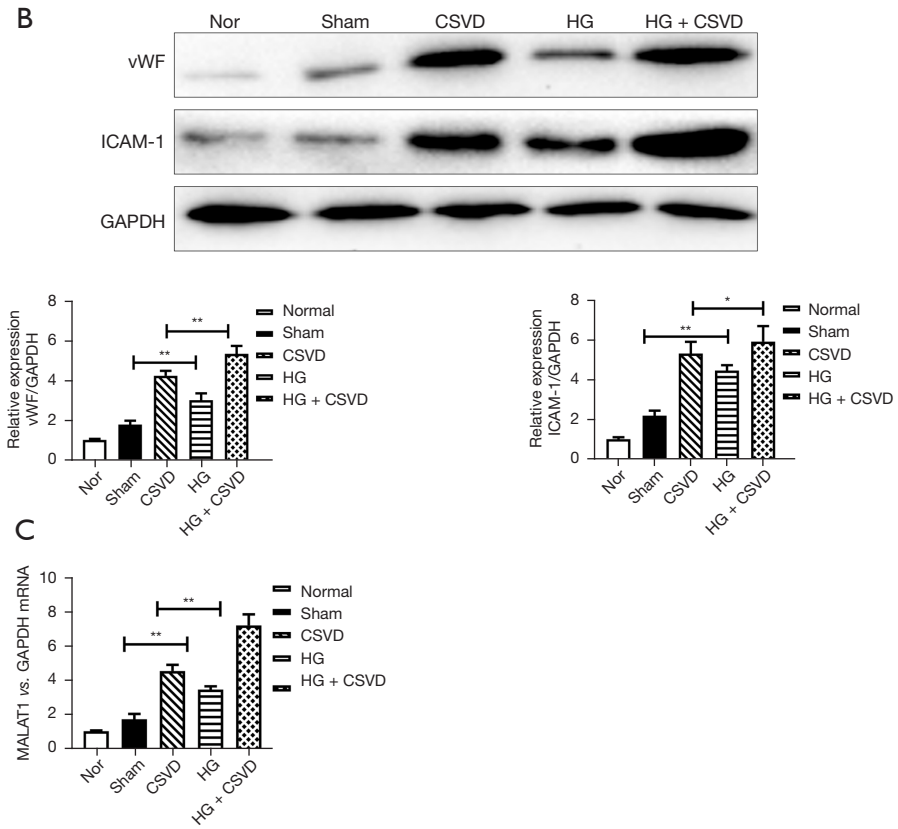

Figure 1 CSVD and hyperglycemia can upregulate the expression of endothelial cell damage markers and cause neurological dysfunction. (A) The Bederson neurologic impairment scale was used to evaluate the degree of neurologic impairment in different treatment groups. The values are expressed as mean ± SD; compared with Sham, *P<0.05, **P<0.01; compared with CSVD, #P<0.05. (B) The expression level of damage markers vWF and ICAM1 were detected by WB. The value in the normal group was regarded as the baseline. The expression trend after standardized treatment was as shown in the figure (n=5, *P<0.05, **P<0.01). (C) The expression of lncRNA MALAT1 in each group was detected by qPCR (n=5, **P<0.01). WB, Western blot; lncRNA, long noncoding RNA; MALAT1, metastasis-associated lung carcinoma transcript 1; Nor, normal; CSVD, cerebral small vessel disease; HG, high glucose; GAPDH, glyceraldehyde-3-phosphate dehydrogenase; vWF, von Willebrand factor; ICAM-1, intercellular cell adhesion molecule-1; SD, standard deviation.

was significantly decreased under HG conditions (HG *vs.* Nor, P<0.01) and upregulated with the inhibition of lncRNA MALAT1 (HG + siMALAT1 *vs.* HG + NC, P<0.01). These results indicated that lncRNA MALAT1 played a role in the nerve cell damage caused by CSVD exacerbated by hyperglycemia through miR-7641.

miR-7641 plays a role in regulating TPR expression and endothelial cell apoptosis

The target genes of miR-7641 predicted in starBase underwent (Gene Ontology, GO) enrichment analysis. The results found that the proteins encoded by the target genes of

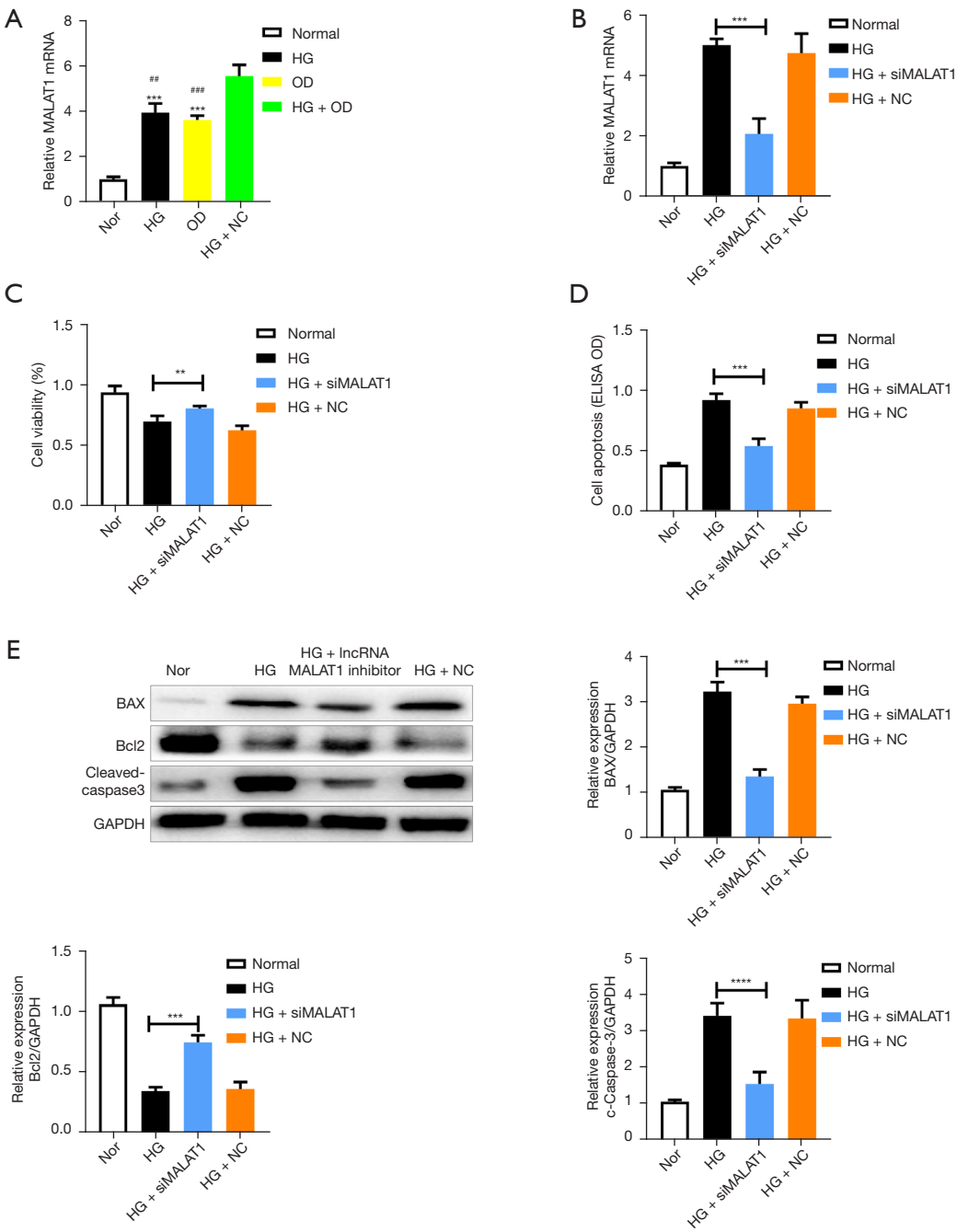

Figure 2 Effect of lncRNA MALAT1 level on cell activity of microvascular endothelial cells. (A,B) The expression level of lncRNA MALAT1 detected by qPCR; ***P<0.001 compared with Nor group; ##P<0.01 compared with HG + OD group, ###P<0.001 compared with HG + OD group; (C) cell activity in different groups detected by MTT; (D) apoptosis detected by ELISA; (E) the expression levels of BAX, BCL2, and c-caspase-3 in each group detected by Western blot. The value in the normal group was regarded as the baseline. The expression trend after standardized treatment was as shown in the figure, HG group compared with MALAT1 interference group, **P<0.01, ***P<0.001, ****P<0.0001, n=3. lncRNA, long noncoding RNA; MALAT1, metastasis-associated lung carcinoma transcript 1. Nor, normal; HG, high glucose; OD, oxygen deprivation; siMALAT1, siRNA MALAT1; NC, negative control; GAPDH, glyceraldehyde-3-phosphate dehydrogenase; BAX, BCL2-associated X; Bcl-2, B-cell lymphoma-2.

A

MALAT1(ReadSeq)	hsa-miR-7641(ReadSeq)	AlignedRegion	FreeEnergy	AlignScore
chr11:65268369-65268385[+]	chr11:104123325-104123344[+]	Query: 5' UGUUGUAGGUU 3' Pair : 3' ACGA-AUCGAA 5'	-6.0	11.5
chr11:65268369-65268385[+]	chr11:104123325-104123367[+]	Query: 5' UGUUGUAGGUU 3' Pair : 3' ACGA-AUCGAA 5'	-18.3	11.5

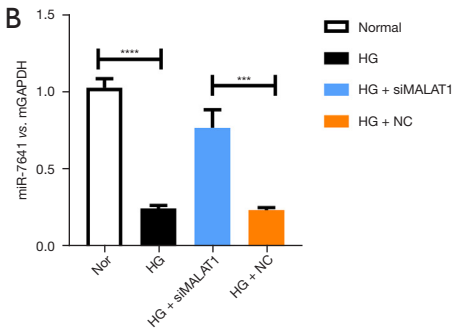

Figure 3 lncRNA MALAT1 interacts with miR-7641. (A) Prediction sites of lncRNA MALAT1 and miR-7641; (B) the expression level of miR-7641 in each group detected by qPCR (n=3, ***P<0.001, ****P<0.0001). lncRNA, long noncoding RNA; MALAT1, metastasis-associated lung carcinoma transcript 1; Nor, normal; HG, high glucose; siMALAT1, siRNA MALAT1; NC, negative control.

miR-7641 were mainly functional components of cells, and that TPR was involved in all enrichment groups (*Figure 4A*). According to starBase, it was found that miR-7641 was involved in the shearing of TPR mRNA (*Figure 4B*). After reviewing relevant literature, we found that TPR protein played an important role in the apoptosis and migration of endothelial cells. Therefore, we speculated that miR-7641 induced endothelial cell apoptosis by promoting the expression of TPR protein. MiR-7641 mimics and miR-7641 inhibitors were used to regulate the activity of miR-7641 in endothelial cells cultured under normal and HG conditions (*Figure 4C,4D*). The results showed that the expression level of TPR mRNA in endothelial cells cultured under normal conditions was significantly increased after treatment with miR-7641 mimic (miR-7641 mimic *vs.* Nor, P<0.01). The expression level of TPR mRNA was significantly reduced in cells cultured under HG conditions after treatment with miR-7641 inhibitor (miR-7641 inhibitor *vs.* HG, P<0.01). The results showed that miR-7641 promoted the expression of TPR. The cell activity in the different experimental groups was detected, and the results showed that the expression level of miR-7641 was positively correlated with cell activity (P<0.01) (*Figure 4E*). Meanwhile, ELISA was used to detect the apoptosis level of cells in different treatment groups (*Figure 4F*), and the results showed that a low level of miR-7641 was associated with a high apoptosis rate. The expression trend of BAX, Bcl2, and c-caspase-3 was detected by WB, with the results showing that the expression of apoptosis-related proteins BAX and c-caspase-3 was more active in the group with lower expression of miR-7641 (*Figure 4G*).

TPR inhibits Akt phosphorylation(p-Akt) and affects the initiation of apoptosis

Some studies have shown that TPR is closely related to apoptosis, and we further explored the mechanism of TPR in the process of apoptosis by regulating the expression of TPR. The results of WB analysis showed that the selected shRNA and overexpressed plasmid played a regulatory role in TPR protein level (*Figure 5A*). It has been reported that TPR promotes Akt phosphorylation (p-Akt), and our results showed that p-Akt inhibited BAX activity by activating GSK3β phosphorylation to inhibit the initiation of endothelial cell apoptosis (*Figure 5B,5C*).

Discussion

Our study showed that lncRNA MALAT1/miR-7641/TPR affected normal vascular function by promoting endothelial

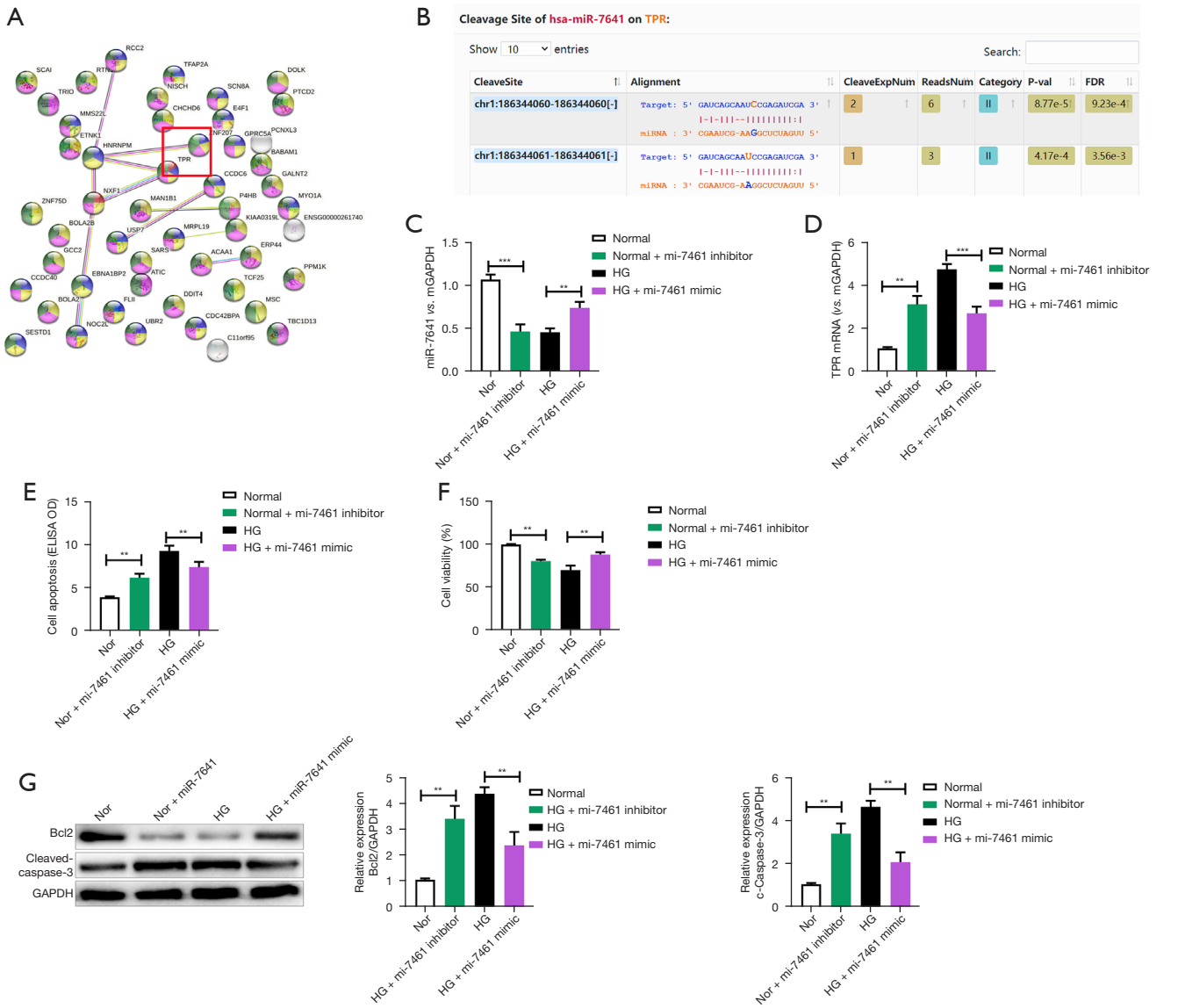

Figure 4 MiR-7641 plays a role in regulating the expression of TPR. (A) MiR-7641 targets gene protein interaction network diagram; each color represents a GO enriched group; (B) starBase analyzed the involvement of miR-7641 in the shearing of TPR mRNA; (C) the expression of miR-7641 in each group detected by RT-qPCR; (D) the expression of TPR in each group detected by RT-qPCR; (E) cell activity detected by MTT; (F) apoptosis detected by ELISA; (G) expression trend of BAX, Bcl2, and c-caspase-3 in each group detected by WB. **P<0.01, ***P<0.001. WB, Western blot; TPR, translocated promoter region. Nor, normal; Nor + miR-7641 inhibitor, normal + miR-7641 inhibitor; HG, high glucose; GAPDH, glyceraldehyde-3-phosphate dehydrogenase; BAX, BCL2-associated X; Bcl-2, B-cell lymphoma-2.

cell apoptosis under hyperglycemia conditions, aggravating CSVD-induced brain damage. However, this pathway is only one of many factors influencing the prognosis of CSVD. LncRNA MALAT1 is widely distributed in blood vessels, skeletal muscle, and myocardial tissues, and it is highly expressed in vascular endothelial cells. It also participates in the processes of proliferation, differentiation, and angiogenesis. In a HG environment, inhibiting the active expression of MALAT1 can maintain the expression level of inflammatory factors such as IL6 and TNF-a within

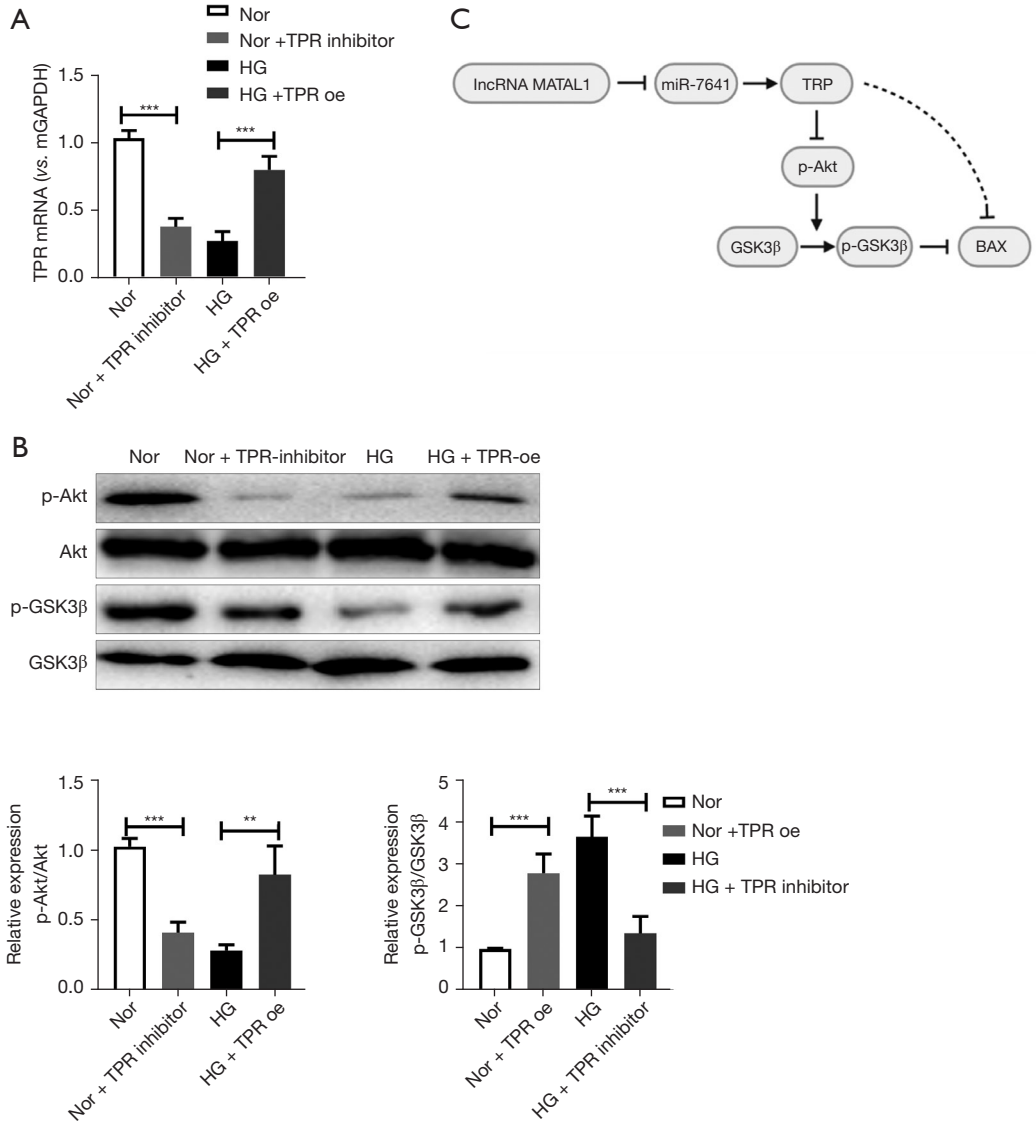

Figure 5 Regulation of TPR expression affects the phosphorylation activity of the Akt pathway. (A) The expression level of TPR protein in each group detected by WB to verify the transfection effect; (B) the expression level of p-Akt/Akt, and p-GSK3β/GSK3β proteins in each group detected by WB; (C) lncRNA MATAL1/miR-7641/TPR pathway diagram. **P<0.01, ***P<0.001. WB, Western blot; TPR, translocated promoter region; lncRNA, long noncoding RNA; MALAT1, metastasis-associated lung carcinoma transcript 1; Nor, normal; Nor + TPR inhibitor, normal + TPR inhibitor; HG, high glucose; TPR oe, TPR over express; GAPDH, glyceraldehyde-3-phosphate dehydrogenase; p-GSK3β, phospho-glycogen synthase kinase-3β.

the normal range, effectively reducing the complications caused by diabetes (22). Other studies have found that lncRNA MALAT1 activated the MEKK3-mediated IκB kinase (IKK)/NF-κB pathway by inhibiting miR-424, thereby promoting the occurrence and development of infantile hemangioma (IH), and also that the inhibition of MALAT1 effectively inhibited tumor growth (23). LncRNA MALAT1 has been found to reduce the expression of breast cancer type 1 (BRCA1) by recruiting *e*nhancer of zeste homolog 2 (EZH2), promoting the phosphorylation of AktT1, and exacerbating the apoptosis and inflammatory response of skeletal muscle cells induced by sepsis (24). Hyperglycemia induces the upregulation of MALAT1 in human lens epithelial cells (HLECs) and promotes

apoptosis and oxidative stress of HLECs by activating the p38 mitogen-activated protein kinase (MAPK) signaling pathway (25).

Knockdown of MALAT1 in diabetic rats has been shown to effectively alleviate the occurrence of capillary lesions, microvascular rupture, and retinal inflammation (26). However, it is important to note that less MALAT1 is not always better. Studies have shown that LncRNA MALAT1 inhibits over-autophagy of endothelial progenitor cells (EPC) induced by coronary heart disease through activation of the mammalian *target* of *rapamycin* (mTOR) signaling pathway (27). Studies have found that MALAT1 silencing induced by gene knockout or pharmacological inhibition promoted the transformation of endothelial cells from proliferative type to migratory type and reduced the growth rate of blood vessels *in vivo* (28). Excessively low level of MALAT1 may increase the occurrence of atherosclerosis, and increased atherosclerosis lesions have been observed in MALAT1-knockout mice. The occurrence of atherosclerosis precursor is mainly caused by the enhanced accumulation of hematopoietic cells (29).

With bioinformatics tools, we analyzed the interaction between miR-7641 and lncRNA MALAT1. As a ribosomal protein regulator, miR-7641 is thought to have 3,500 target genes. The target genes of miR-7641 involve signal transduction, structural components, translation regulation, channel regulation, and antioxidant activity, and they participate in biological localization, stimulus response, development process, immune response, and other physiological processes. Studies have investigated the expression patterns of miR-7641 and its target genes in different cancer cells and clinical cancer patients. It has been confirmed that miR-7641 is a carcinogenic miRNA and plays a role in changing ribosomal protein expression and triggering carcinogenic processes. Overexpression of miR-7641 is seen as a biomarker for the diagnosis of breast cancer and colorectal cancer, and inhibition of miR-7641 expression can improve the efficiency of anticancer drugs. Inhibition of miR-7641 can enhance adriamycin-mediated apoptosis of cancer cells by upregulation of apoptotic molecules caspase 9 (CAS9) and poly ADP RNA polymerase (PARP) and downregulation of anti-apoptotic molecule BCL2 (30). In a study of gastric cancer (GC), it was found that miR-7641 promoted GC cell proliferation and tumor tissue formation through targeted inhibition of AT-rich interactive domain-containing protein 1A (ARID1A) expression (31). Additionally, it has been found that in bladder cancer T24 and SV-HUC-1 cell lines, miR-7641 contributed to cell proliferation by promoting the expression of P16 (32), and that the inhibition of miR-7641 by curcumin effectively promoted the apoptosis of cancer cells.

Nuclear porin TPR is a large α-helix protein and plays a role in RNA and nuclear protein output as a scaffold element of the nuclear pore complex. It has been reported that in duck embryonic fibroblasts, respiratory enterovirus P10.8 induced apoptosis by inhibiting nuclear porin TPR and activating p53 (33). Studies on hepatocellular carcinoma (HCC) have found that TPR was directly involved in the regulation of carcinogenesis, and inhibition of TPR expression inhibited the growth of HCC cells and induced apoptosis (34). TPR is involved in mitosis, including spindle and mitochondrial production. TPR knockdown has been shown to reduce Rac GTPase-activating protein 1 (RACGAP1) phosphorylation and redistribution in the central spindle, affecting cytokinesis in cancer cells and leading to cell stagnation in the growth 2 (G2)/mitosis (M) stage. Our study found that the regulation of miR-7641 affects the expression level of TPR, and TPR acts on the Akt pathway and then affects the process of vascular endothelial cell apoptosis.

Conclusions

In conclusion, the poor prognosis of CSVD is a complex process affected by multiple factors. Clinical data analysis showed that lacunar cerebral infarction, white matter hypersignal, and microhemorrhage were all related to the poor prognosis after surgery, and their indicators could be used to predict the prognosis of patients. In this study, we observed the positive effect of LncRNA MALAT1/miR-7641/TPR on the prognosis of CSVD within the normal expression range. Subsequent studies will further explore the involvement of LncRNA MALAT1/miR-7641/TPR in biological processes, improve the mechanism of brain network damage after CSVD, and provide theoretical support for clinical treatment.

Acknowledgments

Funding: This study was funded by the Qiqihar Medical College Clinical Research Fund Project (QMSI2019L-17).

Footnote

Reporting Checklist: The authors have completed the ARRIVE reporting checklist. Available at https://dx.doi.

org/10.21037/atm-21-5997

Data Sharing Statement: Available at https://dx.doi.org/10.21037/atm-21-5997

Conflicts of Interest: All authors have completed the ICMJE uniform disclosure form (available at https://dx.doi.org/10.21037/atm-21-5997). The authors have no conflicts of interest to declare.

Ethical Statement: The authors are accountable for all aspects of the work in ensuring that questions related to the accuracy or integrity of any part of the work are appropriately investigated and resolved. Animal experiments were approved by the Animal Ethics Committee of Qiqihar Medical University (No. QMU-AECC-2020-66), in compliance with Guidelines for the Ethical Review of Laboratory Animal Welfare (GB/T 35892-2018) for the care and use of animals.

References

1. Liebkind R, Gordin D, Strbian D, et al. Diabetes and intracerebral hemorrhage: baseline characteristics and mortality. Eur J Neurol 2018;25:825-32.
2. Guo R, Chen R, You C, et al. Glucose Levels and Outcome After Primary Intraventricular Hemorrhage. Curr Neurovasc Res 2019;16:40-6.
3. Chang JJ, Khorchid Y, Kerro A, et al. Sulfonylurea drug pretreatment and functional outcome in diabetic patients with acute intracerebral hemorrhage. J Neurol Sci 2017;381:182-7.
4. Irvine H, Male S, Robertson J, et al. Reduced Intracerebral Hemorrhage and Perihematomal Edema Volumes in Diabetics on Sulfonylureas. Stroke 2019;50:995-8.
5. Osei E, Fonville S, Zandbergen AA, et al. Glucose in prediabetic and diabetic range and outcome after stroke. Acta Neurol Scand 2017;135:170-5.
6. Niu C, Chen Z, Kim KT, et al. Metformin alleviates hyperglycemia-induced endothelial impairment by downregulating autophagy via the Hedgehog pathway. Autophagy 2019;15:843-70.
7. Meza CA, La Favor JD, Kim DH, et al. Endothelial Dysfunction: Is There a Hyperglycemia-Induced Imbalance of NOX and NOS? Int J Mol Sci 2019;20:3775.
8. Zheng J, Shi L, Liang F, et al. Sirt3 Ameliorates Oxidative Stress and Mitochondrial Dysfunction After Intracerebral Hemorrhage in Diabetic Rats. Front Neurosci 2018;12:414.
9. Wang W, Wang Y, Long J, et al. Mitochondrial fission triggered by hyperglycemia is mediated by ROCK1 activation in podocytes and endothelial cells. Cell Metab 2012;15:186-200.
10. Lontchi-Yimagou E, Sobngwi E, Matsha TE, et al. Diabetes mellitus and inflammation. Curr Diab Rep 2013;13:435-44.
11. Berbudi A, Rahmadika N, Tjahjadi AI, et al. Type 2 Diabetes and its Impact on the Immune System. Curr Diabetes Rev 2020;16:442-9.
12. Bedini G, Bersano A, Zanier ER, et al. Mesenchymal Stem Cell Therapy in Intracerebral Haemorrhagic Stroke. Curr Med Chem 2018;25:2176-97.
13. Li L, Wang P, Zhao H, et al. Noncoding RNAs and Intracerebral Hemorrhage. CNS Neurol Disord Drug Targets 2019;18:205-11.
14. Zhang J, Dong B, Hao J, et al. LncRNA Snhg3 contributes to dysfunction of cerebral microvascular cells in intracerebral hemorrhage rats by activating the TWEAK/Fn14/STAT3 pathway. Life Sci 2019;237:116929.
15. Chen JX, Wang YP, Zhang X, et al. lncRNA Mtss1 promotes inflammatory responses and secondary brain injury after intracerebral hemorrhage by targeting miR-709 in mice. Brain Res Bull 2020;162:20-9.
16. Zhang HN, Xu QQ, Thakur A, et al. Endothelial dysfunction in diabetes and hypertension: Role of microRNAs and long non-coding RNAs. Life Sci 2018;213:258-68.
17. Włodarski A, Strycharz J, Wróblewski A, et al. The Role of microRNAs in Metabolic Syndrome-Related Oxidative Stress. Int J Mol Sci 2020;21:6902.
18. Sun HJ, Hou B, Wang X, et al. Endothelial dysfunction and cardiometabolic diseases: Role of long non-coding RNAs. Life Sci 2016;167:6-11.
19. Zhang Z, Salisbury D, Sallam T. Long Noncoding RNAs in Atherosclerosis: JACC Review Topic of the Week. J Am Coll Cardiol 2018;72:2380-90.

20. Li H, Zhu H, Ge J. Long Noncoding RNA: Recent Updates in Atherosclerosis. Int J Biol Sci 2016;12:898-910.
21. Xie L, Wang Y, Chen Z. LncRNA Blnc1 mediates the permeability and inflammatory response of cerebral hemorrhage by regulating the PPAR-γ/SIRT6/FoxO3 pathway. Life Sci 2021;267:118942.
22. Lorenzen JM, Thum T. Long noncoding RNAs in kidney and cardiovascular diseases. Nat Rev Nephrol 2016;12:360-73.
23. Li MM, Dong CX, Sun B, et al. LncRNA-MALAT1 promotes tumorogenesis of infantile hemangioma by competitively binding miR-424 to stimulate MEKK3/NF-κB pathway. Life Sci 2019;239:116946.
24. Yong H, Wu G, Chen J, et al. lncRNA MALAT1 Accelerates Skeletal Muscle Cell Apoptosis and Inflammatory Response in Sepsis by Decreasing BRCA1 Expression by Recruiting EZH2. Mol Ther Nucleic Acids 2020;19:97-108.
25. Gong W, Zhu G, Li J, et al. LncRNA MALAT1 promotes the apoptosis and oxidative stress of human lens epithelial cells via p38MAPK pathway in diabetic cataract. Diabetes Res Clin Pract 2018;144:314-21.
26. Liu JY, Yao J, Li XM, et al. Pathogenic role of lncRNA-MALAT1 in endothelial cell dysfunction in diabetes mellitus. Cell Death Dis 2014;5:e1506.
27. Zhu Y, Yang T, Duan J, et al. MALAT1/miR-15b-5p/MAPK1 mediates endothelial progenitor cells autophagy and affects coronary atherosclerotic heart disease via mTOR signaling pathway. Aging (Albany NY) 2019;11:1089-109.
28. Michalik KM, You X, Manavski Y, et al. Long noncoding RNA MALAT1 regulates endothelial cell function and vessel growth. Circ Res 2014;114:1389-97.
29. Cremer S, Michalik KM, Fischer A, et al. Hematopoietic Deficiency of the Long Noncoding RNA MALAT1 Promotes Atherosclerosis and Plaque Inflammation. Circulation 2019;139:1320-34.
30. Reza AMMT, Choi YJ, Yuan YG, et al. MicroRNA-7641 is a regulator of ribosomal proteins and a promising targeting factor to improve the efficacy of cancer therapy. Sci Rep 2017;7:8365.
31. Yang Y, Yin ZX, Wang ZY, et al. miR-7641 depletion suppresses proliferation of gastric cancer cells by targeting ARID1A. Anticancer Drugs 2020;31:368-76.
32. Wang K, Tan SL, Lu Q, et al. Curcumin Suppresses microRNA-7641-Mediated Regulation of p16 Expression in Bladder Cancer. Am J Chin Med 2018;46:1357-68.
33. Wang Q, Huang WR, Chih WY, et al. CDC20 and molecular chaperone CCT2 and CCT5 are required for the Muscovy duck reovirus p10.8-induced cell cycle arrest and apoptosis. Vet Microbiol 2019;235:151-63.
34. Yang XM, Cao XY, He P, et al. Overexpression of Rac GTPase Activating Protein 1 Contributes to Proliferation of Cancer Cells by Reducing Hippo Signaling to Promote Cytokinesis. Gastroenterology 2018;155:1233-49.e22.

(English Language Editor: A. Muijlwijk)

Cite this article as: Che F, Han Y, Fu J, Wang N, Jia Y, Wang K, Ge J. LncRNA MALAT1 induced by hyperglycemia promotes microvascular endothelial cell apoptosis through activation of the miR-7641/TPR axis to exacerbate neurologic damage caused by cerebral small vessel disease. Ann Transl Med 2021;9(24):1762. doi: 10.21037/atm-21-5997

